Structural, magnetic and spectroscopic study of a diluted magnetic oxide: Co doped $CeO_{2-\delta}$

2008 J. Phys.: Condens. Matter 20 125222

(http://iopscience.iop.org/0953-8984/20/12/125222)

J. Phys.: Condens. Matter **20** (2008) 125222 (10pp) doi:10.1088/0953-8984/20/12/125222

Structural, magnetic and spectroscopic study of a diluted magnetic oxide: Co doped $CeO_{2-\delta}$

B Vodungbo[1], F Vidal[1,4], Y Zheng[1], M Marangolo[1], D Demaille[1], V H Etgens[1], J Varalda[2], A J A de Oliveira[2], F Maccherozzi[3] and G Panaccione[3]

[1] Institut des NanoSciences de Paris, UMR 7588 CNRS, Universités Pierre et Marie Curie et Denis Diderot, Campus Boucicaut, 140 rue de Lourmel, 75015 Paris, France
[2] Departamento de Fisica, Universidade Federal de São Carlos, 13565-905, S. Carlos SP, Brazil
[3] TASC Laboratory INFM-CNR, in Area Science Park, S.S.14, Km 163.5, I-34012 Trieste, Italy

E-mail: franck.vidal@insp.jussieu.fr

Received 19 November 2007, in final form 21 January 2008
Published 3 March 2008
Online at stacks.iop.org/JPhysCM/20/125222

Abstract

A structural, spectroscopic and magnetic study of Co doped $CeO_{2-\delta}$ diluted magnetic oxide (DMO) thin films grown by pulsed laser deposition is presented. No secondary phase or metallic clusters could be detected. The samples are ferromagnetic at room temperature and epitaxial films display a large magnetic anisotropy with an out-of-plane easy axis. The evolution of the magnetization with temperature did not reveal any superparamagnetic signal related to nanosized clusters, reinforcing the conclusion that the ferromagnetism is intrinsic in this system. The magnetization at saturation has the same magnitude ($\sim$1.4–1.5 μ_B/Co) in epilayers and textured films and shows no clear dependence on the structural quality, contrary to other DMOs. It is also shown that ferromagnetism is not restricted to a particular region of the films, such as the interface. The ferromagnetic signal depends sensitively on the oxygen pressure during growth and post-growth annealing. The valence of Ce and Co was deduced from x-ray spectroscopies, revealing a predominant Co^{2+} state. The origin of ferromagnetism in Co doped $CeO_{2-\delta}$ is discussed in connection with possible charge-compensating defects and existing models describing indirect exchange in DMOs.

(Some figures in this article are in colour only in the electronic version)

1. Introduction

Recent years have witnessed an impressive research effort to grow and characterize new oxide materials as well as to control and tailor their properties. The wide range of peculiar properties that can be found in oxides make them appealing materials for elaborating multifunctional devices. These properties include colossal magnetoresistance [1], coupled electrical and magnetic degrees of freedom in multiferroics [2] and ferromagnetism (FM) at room temperature (RT) in diluted magnetic oxides (DMOs). Concerning the latter class of materials, there have been many reports of RT-FM in various system after the pioneering works of Dietl *et al* that predicted RT-FM in 5% Mn doped p-type zinc blende ZnO [3] and the subsequent discovery of RT-FM in Co doped TiO_2 by Matsumoto *et al* [4]. Systems studied so far include Co doped [4] and Cr doped [5] TiO_2, ZnO doped by Co, Ti, V, Ni, Fe, Mn [6–9], SnO_2 doped by Co, Cr, Mn, Fe, Ni [10–12], Fe doped HfO_2 [13], Cr doped In_2O_3 [14] and Co doped (La, Sr)TiO_3 [15, 16].

In some cases it was shown that the ferromagnetic signal originated from metallic clusters in the host oxide or from nanosized secondary phases [17]. However, ferromagnetism

[4] Author to whom any correspondence should be addressed.

is an intrinsic property of most of these systems, i.e. RT-FM is present in the doped oxide. Some of these DMO systems were found to be ferromagnetic insulators [18], while others are semiconductors. In most cases no clear correlation between ferromagnetism and conduction properties could be established. For materials such as Cr doped TiO_2 or Co doped ZnO, crystalline quality appears to be detrimental for ferromagnetism: films having a higher crystalline quality are less (or not at all) ferromagnetic than textured ones [5, 19, 20]. More intriguing, RT-FM was reported in the so-called 'd^0' systems, i.e. in undoped oxide thin films [21, 22]. As a general trend in these materials, the presence or absence of robust ferromagnetism seems to be closely linked to the number of structural and electronic defects, as witnessed by the sensitivity to the preparation methods and growth conditions.

The mechanisms governing the appearance of the ferromagnetism in DMOs is far from being understood, particularly in the case of insulating DMOs. Short range direct exchange interaction between 3d cations can be ruled out as the dopant concentration is far below the percolation level. Indirect exchange via the charge carriers may operate in some systems but cannot be invoked in the case of insulating systems. Therefore, the mechanisms governing the appearance of a ferromagnetic ground state in insulating DMOs must in some way differ from that operating in diluted magnetic semiconductors such as GaMnAs. Different models or an explanation based on density-functional theory (DFT) calculation have been proposed recently. Concerning 'd^0' systems, DFT calculation show that the existence of defects in a non-stoichiometric oxide can generate a ferromagnetic ground state of the system [23, 24]. Concerning the magnetism of 3d-doped DMOs, Coey *et al* proposed that a mechanism involving bound magnetic polarons and F-centers in the form of charged oxygen vacancies could explain most of the observed experimental trends [25]. More recently, superexchange between 3d dopants and associated oxygen vacancies, that are required to preserve local charge neutrality in the host matrix, has been proposed [26]. A common salient feature of these calculations and models is the primary role of defects, and in particular of oxygen vacancies, to mediate the exchange interaction.

Ceria (CeO_2) is a high dielectric constant rare-earth oxide that could be attractive as a DMO when doped by 3d cations, for several reasons. First, it is a face centered cubic system with a cubic fluorite crystal structure ($Fm3m$ space group) with a lattice constant ($a = 5.411$ Å) that is matched with silicon. Therefore, it could be of great interest for integrating functional oxides on silicon in future spintronics devices. Secondly, ceria can support strong deviation to stoichiometry ($CeO_{2-\delta}$ with $0 < \delta < 0.4$–0.5) while retaining its fluorite structure. Considering the potential role of oxygen vacancies in ferromagnetic exchange in DMOs, it is then interesting to study such a material. In fact, recent studies show that Co doped ceria is ferromagnetic at room temperature [27–30]. We showed recently that RT-FM in this DMO is strongly dependent on the oxygen pressure during growth and annealing and that Co doped $CeO_{2-\delta}/SrTiO_3(001)$ epilayers display a large magnetic anisotropy with an out-of-plane easy axis [28].

In this paper, we present an extended study of the structure, composition and magnetic properties of Co doped $CeO_{2-\delta}$ RT-FM insulating DMOs, following our previous report [28]. Films grown on oxidized Si and $SrTiO_3(001)$ substrates are investigated and the results are organized as follows: in section 2, the different experimental techniques used are described; section 3 is devoted to structural characterization; the magnetic properties are presented in section 4; section 5 concerns the spectroscopic investigation of the samples; the results are discussed in connection with existing models of ferromagnetic ordering in DMOs in section 6.

2. Experimental details

The Co doped $CeO_{2-\delta}$ thin films were grown by pulsed laser deposition (PLD). Growth of the samples was carried out in a PLD set-up using a KrF excimer laser operating at 248 nm and 2 Hz with a fluence of 3 J cm^{-2} and a high-vacuum (10^{-7} mbar) chamber. The growth temperature was 650 °C. Two types of targets were used: CeO_2 and CoO. The laser shots sequence was set so as to adjust the percentage of Co in the films. The resulting composition was checked afterward using Rutherford backscattering. Hereafter we present results obtained for a 4.5% Co atomic content. The thickness of the films was around 400 nm, unless otherwise indicated. For each type of substrate, two kinds of samples were studied: samples grown under an oxygen-rich atmosphere (5×10^{-2} mbar) and samples grown under a vacuum.

X-ray diffraction (XRD) was carried out using a Philips X'Pert MRD four-circle diffractometer with Cu Kα radiation and a graphite monochromator in front of the detector.

High resolution transmission electron microscopy (HRT EM) was performed at IMPMC, Paris, France, using a JEM 2100F field emission microscope operating at 200 kV with a 0.18 nm point resolution. The microscope was equipped with a Gatan GIF electron spectrometer.

X-ray photoemission spectroscopy (XPS) and x-ray absorption spectroscopy (XAS) were performed at the Advanced Photoelectric Effect Experiments (APE) beamline at the Elettra Synchrotron, Trieste, Italy. The available energy range is 140–1500 eV in the soft x-ray range.

Magnetic measurements were carried out using a Quantum Design superconducting quantum interference device (SQUID) magnetometer and an alternating gradient field magnetometer (AGFM). SQUID measurements were performed at the Université Pierre et Marie Curie, Paris, France and the Universidade Federal de São Carlos, S. Carlos, Brazil. AGFM measurements were performed at the Unité Mixte de Physique CNRS/Thalès (UMR 137), Palaiseau, France.

3. Structural properties

3.1. Films grown on oxidized Si

X-ray diffraction experiments show that the films are not epitaxially grown but textured with a predominant orientation. This preferential orientation depends on the growth conditions:

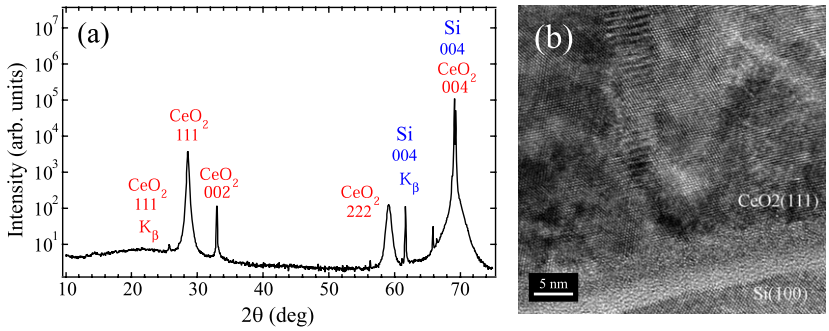

Figure 1. (a) X-ray diffraction θ–2θ scan of 4.5% Co doped $CeO_{2-\delta}$ film grown on oxidized Si. (b) TEM image of 4.5% Co doped $CeO_{2-\delta}$ film grown on oxidized Si.

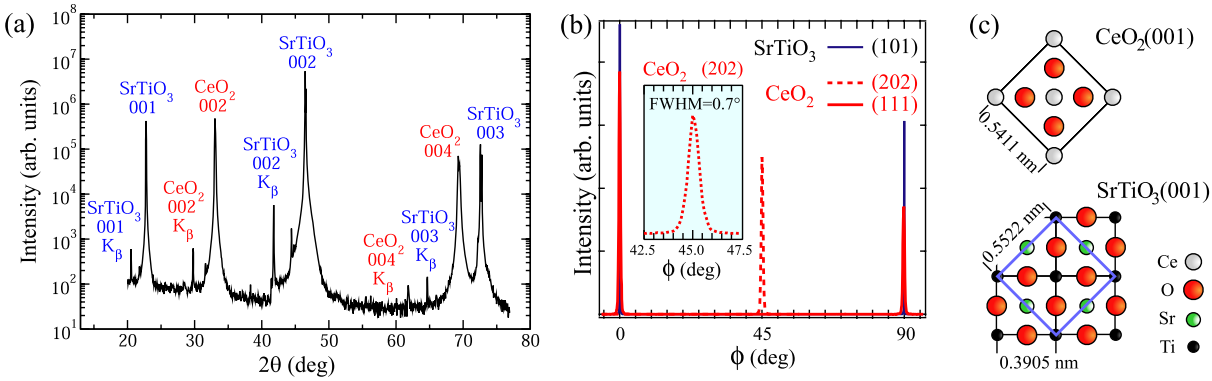

Figure 2. (a) X-ray diffraction θ–2θ scan of 4.5% Co doped $CeO_{2-\delta}$ film grown on $SrTiO_3(001)$. (b) ϕ-scan of 4.5% Co doped $CeO_{2-\delta}$ film grown on $SrTiO_3(001)$. (c) Scheme of the Co doped $CeO_2/SrTiO_3(001)$ epitaxy.

in films grown under vacuum the (111) plane is parallel to the substrate surface, as shown by the diffraction data reproduced in figure 1(a), and under oxygen the (001) plane is parallel to the substrate surface. Such a dependence of the orientation on the growth atmosphere has already been reported for undoped CeO_2 films [32]. No secondary phase could be detected by XRD. The textured structure of the film is evident in TEM images such as the one depicted in figure 1(b).

3.2. Films grown on $SrTiO_3$

The θ–2θ scan of a 4.5% Co doped $CeO_{2-\delta}$ film grown on $SrTiO_3(001)$ is displayed in figure 2(a). No peaks other than $(00l)$ reflections of CeO_2 and $SrTiO_3$ could be detected, revealing a single phase with the [001] direction perpendicular to $SrTiO_3(001)$. ϕ-scans enabled the determination of the epitaxial relationship. As shown in figure 2(b), the (111) reflections of the films coincide with the (101) reflections of $SrTiO_3$ and are located at 0° and 90°. The (202) reflections of CeO_2 also exhibit a 90° periodicity and are shifted by 45° with respect to $SrTiO_3(101)$ reflections. This indicates a 45° rotation in the (001) plane of the substrate of the unit cell of the film with respect to the $SrTiO_3$ unit cell, as sketched in figure 2(c). Such a rotation reduces the lattice mismatch ($a = 3.905$ Å for $SrTiO_3$ and $a = 5.411$ Å for CeO_2) to 2% and, in this configuration, the oxygen sublattices of the film and the substrate match. The deduced epitaxial relationship is then $(001)_f \parallel (001)_s$, $[100]_f \parallel [1\bar{1}0]_s$, $[010]_f \parallel [110]_s$, where 'f' and 's' subscripts stand for film and substrate, respectively. This relationship is identical to the one found in a previous study of undoped CeO_2 growth on $SrTiO_3(001)$ substrates [33]. The full width at half maximum (0.7° for the film, 0.1° for the substrate) of the ϕ-scan peaks (see inset in figure 2(b)) indicates a good crystalline quality of the epilayer.

Information on mass density and surface roughness of the films was also obtained from x-ray reflectivity measurements. The measured critical angle on all films analyzed is fully consistent with a CeO_2 bulk density of 7.65 g cm^{-3}. From the shape of the falling edge beyond the critical angle, a surface roughness of 3.0 Å ± 0.1 Å is deduced for Co doped $CeO_{2-\delta}$ films grown under vacuum. It should be noticed that the surface roughness remains the same when decreasing the thickness from 400 to 34 nm.

The crystalline quality was further checked using TEM. A large scale image reveals a homogeneous film free from extended defects, as shown in figure 3(a). No clusters could be detected in the film. Figures 3(b) and (c) display high resolution images of the interfacial region. The interface between the epilayer and $SrTiO_3$ is sharp and, again, no clustering or increased density of extended structural defects could be detected. Local electron energy loss spectra acquired at various spots in the film indicate a uniform distribution of Co in the $CeO_{2-\delta}$ matrix and show no evidence of clustering. Due

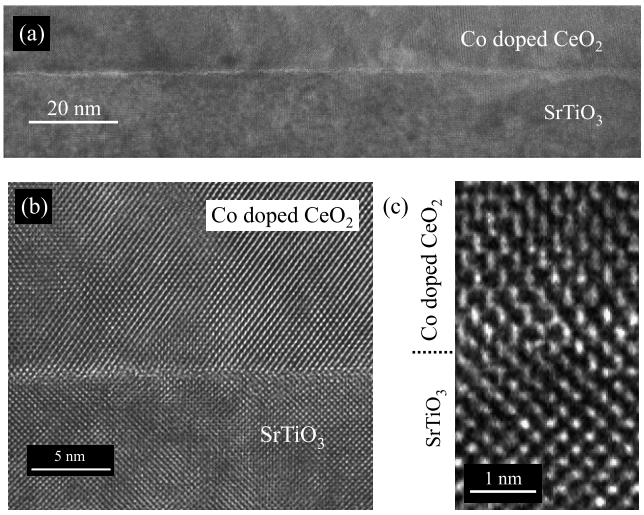

Figure 3. (a) Large scale TEM image of the Co doped CeO_2 epitaxial thin film. (b) High resolution TEM image of the interface between Co doped CeO_2 and $SrTiO_3$. (c) Zoom on the interfacial region.

to a low signal level, it was not possible to determine the charge state of the Co ions from the electron energy loss spectra.

4. Magnetic properties

4.1. Films grown on oxidized Si

No ferromagnetic signal could be detected in undoped samples. As shown by the hysteretic cycles in figure 4, the 4.5% doped samples grown under vacuum are clearly ferromagnetic at 300 K. The Curie temperature was found to be higher than 400 K. The evolution of the magnetic properties at higher temperatures was not investigated since it requires control of the atmosphere or capping the samples in order to avoid any evolution (such as oxygen release that can happen in CeO_2). The magnitude of the FM signal is strongly dependent on the oxygen content of the growth atmosphere. The saturation magnetization drops markedly for samples grown under 5×10^{-2} mbar of oxygen when compared to samples grown under vacuum (figure 4(a)). A similar decrease of the FM was observed when annealing samples grown under vacuum in oxygen-rich conditions ($T = 650\,^{\circ}\mathrm{C}, 5\times10^{-2}$ mbar), as shown in figure 4(b). From the saturation magnetization the magnetic moment per Co ion is $M_{Co^{2+}} = 1.4\pm0.2\ \mu_B$ for samples grown under vacuum.

4.2. Films grown on $SrTiO_3$

As shown by figure 4(c), epilayers grown on $SrTiO_3$ were also found to be ferromagnetic at room temperature. The measured magnetic moment per Co ion is $M_{Co^{2+}} = 1.5 \pm 0.2\ \mu_B$ and T_C is higher than 400 K. Figures 4(c) and (d) illustrate the effect of oxygen content during growth or post-growth annealing on the ferromagnetic response of the epilayers. As in the case of films grown on Si, an oxygen-rich atmosphere during growth or thermal treatment leads to a drastic reduction of the saturation magnetization. Field-cooled (FC) and zero-field-cooled (ZFC) data obtained for films grown under vacuum are presented in figures 5(a) and (b) for an out-of-plane applied magnetic field of 700 and 5000 Oe, respectively. No signals related to an assembly of superparamagnetic particles were observed in the temperature range investigated, reinforcing the conclusion that clustering at the nanometer scale of a FM secondary phase is not at the origin of RT-FM in the samples.

The inset in figure 5(c) shows details of the hysteretic cycles at lower fields for in-plane and out-of-plane applied

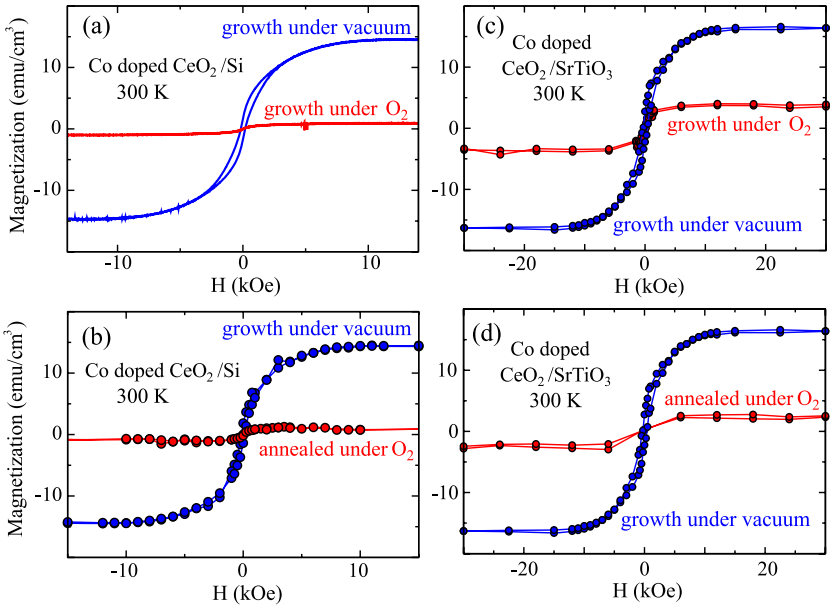

Figure 4. (a) Magnetization cycles measured with AGFM (in-plane magnetic field) at 300 K obtained for a 4.5% Co doped $CeO_{2-\delta}$ film deposited on Si for samples grown under vacuum and under oxygen-rich conditions. (b) Magnetization cycles (in-plane magnetic field) measured with a SQUID magnetometer at 300 K obtained for a 4.5% Co doped $CeO_{2-\delta}$ film deposited on Si under vacuum before and after annealing under oxygen-rich conditions. (c), (d) The same as (a), (b) for epilayers grown on $SrTiO_3$(001) (SQUID).

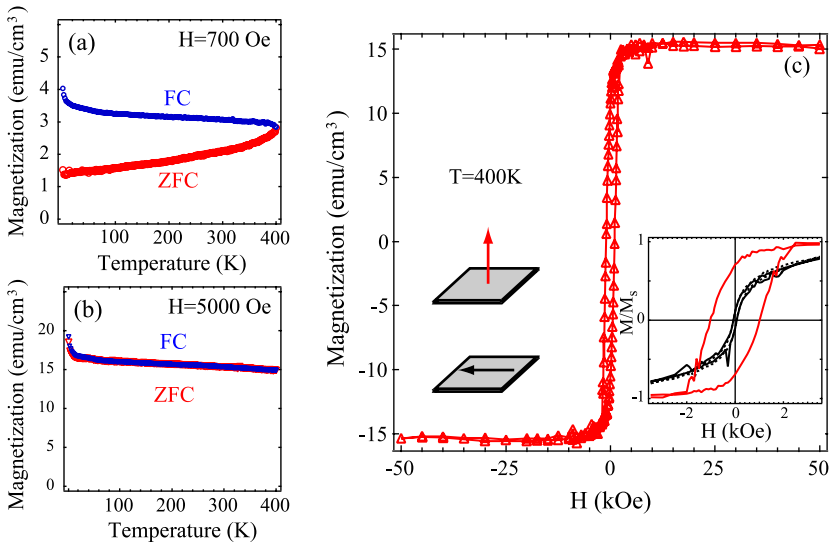

Figure 5. (a) Zero-field-cooled (ZFC) and field-cooled (FC) data for a 4.5% Co doped $CeO_{2-\delta}$ epitaxial film on $SrTiO_3$ obtained for $H = 700$ Oe. (b) The same as (a) for $H = 5000$ Oe. (c) Magnetization cycles measured with a SQUID magnetometer (out-of-plane magnetic field) as a function of the magnetic field obtained for a 4.5% Co doped $CeO_{2-\delta}$ epitaxial film (grown under vacuum) on $SrTiO_3$. The inset is a zoom of the hysteretic region, showing cycles for out-of-plane in and in-plane (two in plane directions at 45° were probed) magnetic field. Red (gray) line: magnetization for an out-of-plane applied magnetic field. Black lines: magnetization for an in-plane applied magnetic field.

magnetic fields. These data clearly reveal a strong magnetic anisotropy. The absence of any marked in-plane anisotropy implies that we have a dominant uniaxial anisotropy with an easy axis perpendicular to the film plane. The magnetocrystalline anisotropy in a cubic system cannot account for a uniaxial anisotropy. Moreover, in a magnetic film of thickness 400 nm, the shape anisotropy favors an in-plane magnetization, i.e. a hard axis perpendicular to the film plane. Therefore the shape anisotropy can also be discarded. In the case of $Ga_{(1-x)}Mn_xAs$, the most studied diluted magnetic material, it has been shown that the magnetic anisotropy depends both on the strain in the film and on the doping level [34]. In the case of Co doped $CeO_{2-\delta}$ the origin of magnetic anisotropy may lie in similar mechanisms. In fact, the lattice mismatch between CeO_2 and $SrTiO_3$ and the local distortion due to oxygen vacancies could be the source of residual strain in the epilayer. From XRD data we evaluate an upper limit of 0.2% difference between the in-plane and out-of-plane lattice parameter of the 400 nm films on $SrTiO_3$. This residual strain could lead to the observed anisotropy. In $Ga_{(1-x)}Mn_xAs$, the charge carriers mediate indirect ferromagnetic interactions and their concentration influences the magnetic anisotropy. We suspect that in the case of Co doped $CeO_{2-\delta}$, the indirect FM coupling mechanism may be related to the presence of oxygen vacancies or other electronic defects (see section 6). The concentration and distribution of such species may also have an impact on the magnetic anisotropy in the present system. However, further work is needed to confirm these hypotheses. It is anticipated that further studies on (001) perovskite-like substrates with *ad hoc* lattice parameter and on epilayers with different Co concentration could help to clarify this point and may enable tailoring of the magnetic anisotropy. A detailed study of the anisotropic behavior is outside the scope of this paper.

5. Spectroscopic study

The Co L_2–L_3 XAS spectra of 4.5% Co doped $CeO_{2-\delta}$, CoO (with a 2+ valence of Co) and Co metal are displayed in figure 6. We observe that the spectrum of the DMO shows more resemblance to the spectrum of the CoO reference sample. Comparison with the spectrum of $LiCoO_2$, published in the literature, with Co ions in the 3+ charge state, is also unfavorable: the characteristic low energy broad shoulder present in the L_3 component of the Co^{3+} XAS spectrum of $LiCoO_2$ is absent in the present measurement [35]. The fact that the Co XAS spectrum of the sample looks relatively similar, in terms of line position and line shape, to that of CoO gives a strong indication that most of the Co ions are in the divalent Co^{2+} valence state in Co doped $CeO_{2-\delta}$.

As shown by Skorodumova *et al*, the ability of ceria to release oxygen proceeds via the creation of oxygen vacancies accompanied by electron localization processes on the two neighboring Ce ions in the lattice. This leads to a Ce^{3+} ($4f^1$) state instead of Ce^{4+} ($4f^0$) in stoichiometric CeO_2 [31]. According to this picture, the determination of the Ce^{3+} content in the film could lead to an estimation of the oxygen vacancy content. However, the incorporation of Co ions in the lattice can also influence the creation of oxygen vacancies: for example, the existence of Co^{2+}_{Ce} in the lattice would require local charge compensation. This could be realized in different ways. One possibility is to form a (V^{2+}_O, Co^{2+}_{Ce}) complex associating the Co ion with an oxygen vacancy. In this case, neighboring Ce ions can retain their 4+ charge state. Therefore, considering the potential role played by oxygen vacancies, it would be helpful to determine the charge state of Ce ions in order to get a better understanding of the microscopic details governing the magnetic exchange. Thus we have recorded XAS spectra at the M_4–M_5 edges of Ce.

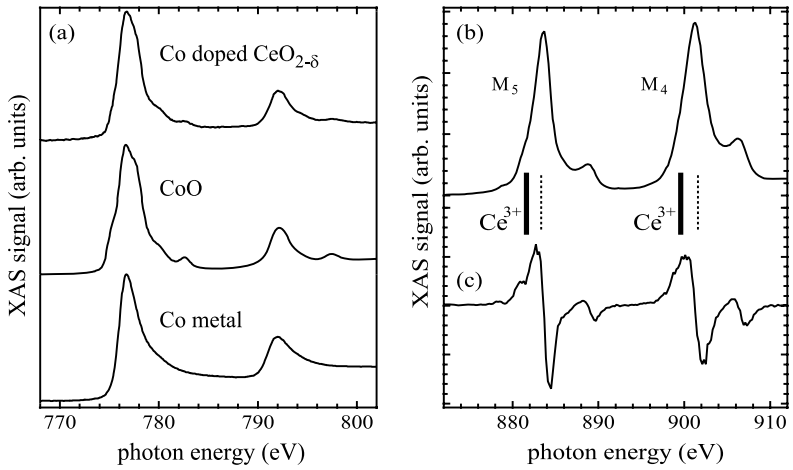

Figure 6. (a) CoL_2–L_3 XAS spectra of 4.5% Co doped $CeO_{2-\delta}$, CoO and Co. (b) M_4–M_5 XAS spectrum of Co doped $CeO_{2-\delta}$ grown on Si. (c) Derivative of the absorption spectra depicted in (b).

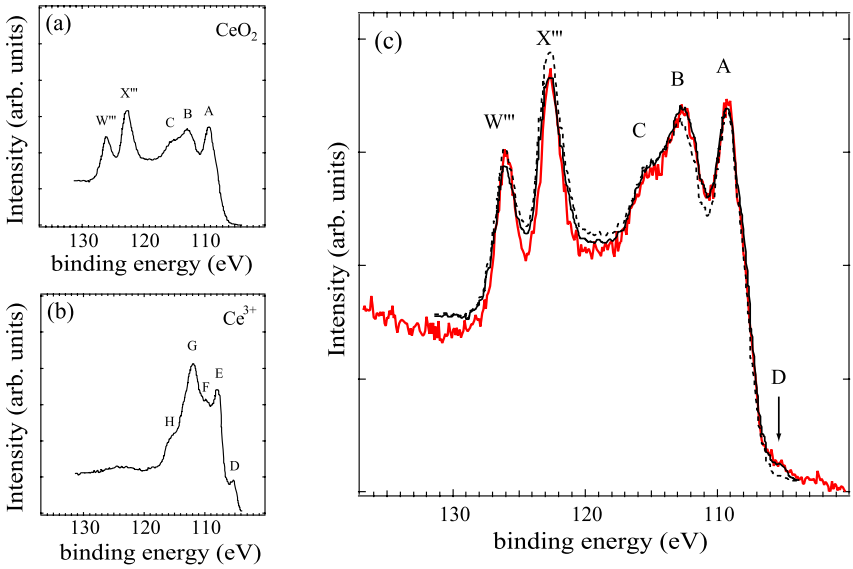

Figure 7. (a) XPS spectrum of CeO_2 in the Ce 4d spectral region. (b) XPS spectrum of Ce^{3+} in the Ce 4d spectral region. (Parts (a) and (b) adapted from [37] with permission from Elsevier.) The characteristic spectral features in (a) and (b) are labeled with the same nomenclature as used in [37]. (c) Thick red (gray) line, Ce 4d XPS spectrum of Co doped $CeO_{2-\delta}$ grown on Si; thin black dashed line, scaled CeO_2 spectrum; thin black line, linear combination of the spectra in (a) and (b).

Figure 6(b) shows an XAS spectrum of Co doped $CeO_{2-\delta}$ grown on Si in the M_4–M_5 spectral region. This spectrum appears similar to the one for an undoped CeO_2 sample [36]. Also shown in figure 6(b) are the position of M_4 and M_5 white lines of Ce^{3+} (thick vertical bars) of metallic Ce [36]. These white lines are shifted towards lower photon energies from ∼2 eV with respect to their position in CeO_2 (vertical dashed lines). A closer look on the spectrum in figure 6(b) reveals the existence of a shoulder on the low energy tail of the M_5 white line. The appearance of such a feature is best seen in the derivative of the spectrum (figure 6(c)). Concerning the M_4 white line, it is possible that another, less intense, component lies at lower energy, although such a feature is not resolved in the spectrum. Considering that M_4 and M_5 white lines are shifted towards lower photon energies for Ce^{3+}, this indicates that a minority of Ce ions are in the 3+ state in the sample. However, it is not possible to evaluate quantitatively the fraction of Ce^{3+} ions from these XAS measurements. Therefore, XPS was also employed.

XPS spectroscopy of Ce 4d can also be used to determine the Ce^{3+} content in CeO_2 samples [37]. Ce 4d photoemission spectra of Ce^{4+} and Ce^{3+} are markedly different, as illustrated in figures 7(a) and (b) where spectra taken from [37] have been reproduced. The characteristic spectral features in (a) and (b) are labeled with the same nomenclature as used in [37]. The overall aspect of the Co doped $CeO_{2-\delta}$ photoemission spectrum displayed in figure 7(c) is quite similar to the one of spectrum (a). A, B, C, X‴ and W‴ spectral components are clearly identified and have relative spectral weights reminiscent of the pure CeO_2 spectrum, indicating a predominant Ce^{4+} charge state in the sample. However, a closer inspection of this spectrum reveals minute characteristic differences from

spectrum (a). This is illustrated in figure 7(c), where scaled spectrum (a) has been superimposed upon (c). For example, peak X‴ has a lower intensity in the doped sample than in pure CeO_2. The spectral shape is also quite different in the vicinity of the B component. Moreover, the photoemission intensity in the spectral region of band D of Ce^{3+} is higher in the spectrum of the doped sample, as shown by the vertical arrow in figure 7(d). To account for these variations in the spectral shape, the spectrum of Co doped $CeO_{2-\delta}$ was modeled as a linear combination of CeO_2 (Ce^{4+}) and Ce^{3+} spectra: $I = (1-x)I_{xps}(Ce^{4+}, 4d)+xI_{xps}(Ce^{3+}, 4d)$. This has allowed us to reproduce the spectrum of Co doped $CeO_{2-\delta}$ for $x = 0.1$. As shown in figure 7(d), the agreement is excellent. However, it is not possible to conclude that the concentration of Ce^{3+} actually reaches 0.1 within the bulk of the samples because of the XPS surface sensitivity: the samples are probed within the penetration depth only. Nevertheless, the results indicate clearly that a sizeable fraction of the Ce ions are in the trivalent Ce^{3+} charge state in the 4.5% Co doped samples.

6. Discussion

The combined structural and magnetic (no blocking temperature observed up to 400 K) analysis presented before indicates clearly that RT-FM is intrinsic in the Co doped $CeO_{2-\delta}$ films. This observation is not related to metallic Co clusters in a superparamagnetic state, or to the presence of nanometric secondary phases or of extended structural defects in the films and at the interface with the substrate. The formation of a Co rich layer at the surface of the film, as has been observed in Co doped HfO_2 [38], or at the interface can also be ruled out from high resolution TEM and x-ray reflectivity measurements.

Concerning the fact that FM is not related to metallic Co clusters, it is worthwhile making the following remarks. First, if the magnetic signal was related to a superparamagnetic assembly of Co clusters, then the blocking temperature T_B would be higher than 400 K. Taking $T_B \sim 500$ K, we can evaluate the average Co particle volume V using the relation $KV \sim 25k_BT_B$, where K is the anisotropy constant. If we take $K = 4.1 \times 10^5$ J m^{-3} for cobalt [39], we get $V \sim 421$ nm^3, corresponding to a mean diameter $D \sim 7.5$ nm. Such clusters would be clearly seen in high resolution TEM images, and this is not the case here. Another point deserves to be underlined: metallic Co clusters should be oriented with their easy axis lying out of plane in order to explain the anisotropic magnetic response of the films. In such a case, the anisotropy field H_a should be close to 6 kOe, the value of bulk Co [39]. This is not what is observed. From the initial slopes of M versus H data (see figure 4 and inset in figure 5(c), for H applied in plane), $H_a \sim 1$ kOe. Such a value is clearly too low to be consistent with an assembly of oriented Co clusters. To end these remarks, the spectroscopic results combined with the value of the saturation magnetization argue against an explanation invoking Co particles as the origin of the magnetic behavior. From magnetic measurements, we get 1.5 μ_B/Co at saturation in the films. In bulk Co, this value amounts to 1.7 μ_B. Therefore, if the magnetic signal was linked with metallic Co particles, about 90% of the cobalt should be in a metallic state. Such a high proportion should be readily detected by XAS at Co L_2–L_3 edges. Again, this is not the case. Thus, in the light of the preceding remarks, Co metal can be safely eliminated as the source of magnetism.

Comparison between the results obtained for samples grown on oxidized Si and $SrTiO_3(001)$ substrates can be made in order to evaluate the impact of extended structural defects on the magnetism. The fact that there is no significant difference in terms of saturation magnetization between epitaxial samples of good crystalline quality and textured ones is at variance with what has been observed for other DMOs, notably Cr doped TiO_2 [5]. For this particular system, it is believed that extended structural defects play a primary role in the exchange process leading to the appearance of FM. Our findings suggest that this is not the case for the Co doped $CeO_{2-\delta}$ films.

Recent studies on PLD grown doped ZnO show that the magnetization scales with the surface of the sample and that the total moment does not depend sensitively on the films thickness, suggesting an interfacial origin of FM in such samples [8]. In order to examine this possibility, we have grown thinner Co doped films on $SrTiO_3(001)$. For a thickness of 34 nm, the magnetization at saturation per surface unit is about 13 times smaller than that of 400 nm thick films and corresponds also to 1.5 μ_B/Co. This indicates clearly that, for the present system, FM is not restricted to a particular region but exists in the whole film.

No FM signal could be detected in undoped films, contrary to what has been reported in the literature concerning some sub-stoichiometric oxides (mostly HfO_2 and TiO_2) thin films. In the present case, the FM signal is not related to a 'd^0' ferromagnetism that would be enhanced by the introduction of 3d dopants, as is sometimes postulated for other systems. The appearance of RT-FM is rather related to Co ions and possibly to FM-mediating defects, the latter not being sufficient to explain RT-FM.

In order to determine whether Co is incorporated in the CeO_2 host or not, we have measured the variation of the CeO_2 lattice parameter as a function of the Co atomic percentage (x_{Co}) in the epitaxial films grown under vacuum. The data are depicted in figure 8(a). The value of the lattice parameter was deduced from x-ray diffraction (using the (004) reflection of Co doped $CeO_{2-\delta}$ in comparison with the (003) reflection of $SrTiO_3$). The Co content was either measured by RBS or extrapolated. The extrapolation was based on the linear relation between the nominal content and the measured composition deduced from RBS measurements. There is a clear dependence of the lattice parameter on x_{Co}, indicating Co incorporation in the CeO_2 lattice up to ~8%. The determination of the position of Co ions in the lattice requires additional experiments. However, it is reasonable to assume Co^{2+}_{Ce} substitutional occupancy since the ionic radii of Co^{2+} and Ce^{4+} are close for coordination 8: 0.9 Å and 0.97 Å, respectively. The presence of Co^{2+}_{Ce} would induce the creation of charge compensating defects such as oxygen vacancies and Ce^{3+}. This latter species would be responsible for the increase in the lattice parameter [40].

The measured saturation magnetization (M_s) values as a function of Co content are plotted in figure 8(b). M_s shows a

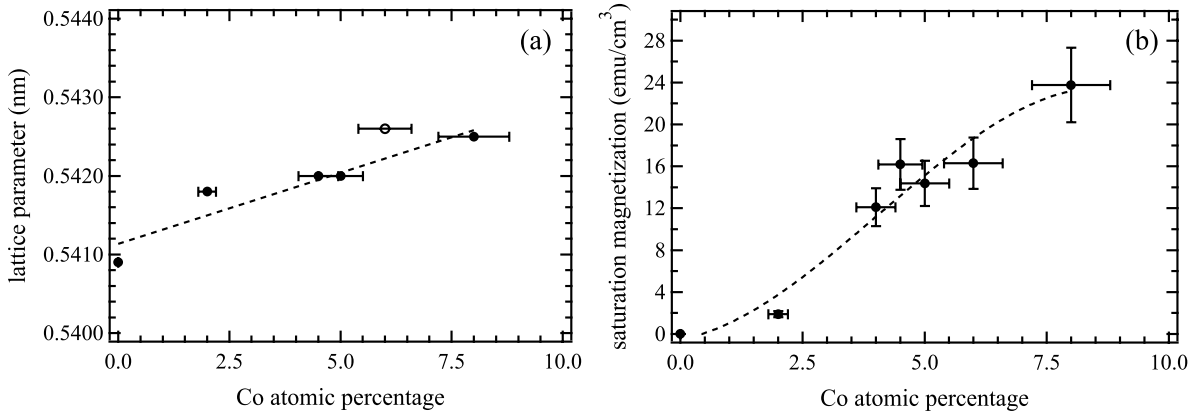

Figure 8. (a) Measured CeO_2 lattice parameter as a function of Co atomic percentage for samples grown under a vacuum (black disks, Co percentage measured by RBS; circles, extrapolated Co percentage—the extrapolated percentage is deduced from the nominal composition given the relation between this latter composition and the actual percentage measured by RBS). The dashed line is a linear fit taking into account the data involving RBS measurements. (b) Saturation magnetization as a function of Co atomic percentage for samples grown under a vacuum. The dashed line is a guide to the eye.

clear dependence on the Co atomic percentage and increases as x_{Co} increases. Such a behavior is consistent with Co ions being involved in the magnetic response. Above $x_{Co} \sim 4\%$, the moment at saturation per Co is roughly constant (1.4–1.5 $\pm$ 0.2 μ_B/Co^{2+}) and lies between the low-spin moment and the high-spin moment of Co^{2+}. Our results differ from those reported by Tiwari *et al* with a giant magnetic moment [27]. The reason for this discrepancy is unclear. We note that the measured moments do not need to call for unquenched orbital moments of Co ions to be explained. For $x_{Co} = 2\%$, the moment per Co is lower ($\sim$0.4 μ_B) than the one found at higher Co content ($x_{Co} > 4\%$). This could be due to the fact that only a reduced fraction of Co ions exhibits ferromagnetic order at low Co concentration, probably because the mean Co–Co distance is higher than the range of ferromagnetic interactions.

Indeed, at the doping level studied, Co ions are too far from each other to enable direct, short range, ferromagnetic coupling between them. Conductivity measurements revealed that as-grown and annealed Co doped CeO_2 samples are insulating. Therefore, carrier mediated exchange mechanisms can be ruled out in the present case. Simple ferromagnetic superexchange, which has been predicted to occur in highly doped (25%) $Ti_{(1-x)}Co_xO_2$ [41], cannot account for the observed FM in the range of doping investigated here. Obviously, one has to invoke additional species in the exchange process. The sensitivity of ferromagnetism on the oxygen content of the growth or annealing atmosphere, as shown by the results of section 4, points naturally to oxygen vacancies. Indeed Coey *et al* proposed recently that singly charged oxygen vacancies (F-centers) forming bound magnetic polarons with the 3d dopants might be involved in the ferromagnetic coupling [25]. Due to the high dielectric constant generally found in oxides, such defects have a large radius and their percolation, happening well before the percolation of the magnetic impurities, ensures the long range interaction between 3d ions. This model applies in the case where singly charged vacancies exist. A recent hybrid density-functional study by Patterson showed that singly charged O vacancies promote ferromagnetic exchange but are not stable in $Zn_{(1-x)}Co_xO$ [42]. Pairs of singly charged vacancies are predicted to dissociate into neutral and doubly charged vacancies, and these latter species do not promote ferromagnetic exchange. Thus, singly charged oxygen vacancies may not be the likely cause of the observed FM in $Zn_{(1-x)}Co_xO$. In this compound, Co ions substitute for Zn ions and both species have a 2+ charge state. Therefore, Co doping does not necessarily imply the formation of vacancies. The situation is different in the case of Co doped $CeO_{2-\delta}$: the existence of aliovalent Co_{Ce}^{2+} species implies the formation of charge compensating defects as already stated in the previous section. The simplest possibility is the formation of a (V_O^{2+}, Co_{Ce}^{2+}) complex associating the Co ion with an oxygen vacancy (see figure 9(a)). This type of defect will be labeled 'complex I' in the following discussion. Another possibility is the creation of defects with the formation of two oxygen vacancies in the vicinity of Co_{Ce}^{2+}, each transferring one electron to Co^{4+} in order to form Co^{2+} and one electron to neighboring Ce^{4+} ions leading to the formation of two Ce^{3+} ions (see figure 9(b)). This can be viewed as a process mixing the process leading to complex I and the process leading to Ce^{3+} ions by electron localization in the Ce 4f orbitals during the formation of an oxygen vacancy in CeO_2 (see figure 9(c)) [31]. Hereafter we label this kind of defect 'complex II'. Neither complex I nor complex II can be involved in the formation of F-center magnetic polarons. Therefore, other possibilities have to be explored to account for RT-FM in Co doped $CeO_{2-\delta}$.

A recent theoretical work suggests that the FM ground state of insulating Co doped TiO_2 could be explained by superexchange coupling between (V_O^{2+}, Co_{Ti}^{2+}) complexes [26]. In this model, the extended empty states of vacancies form a band below the percolation threshold of the magnetic dopants, ensuring long range ferromagnetic interaction between magnetic impurities via two V_O^{2+} centers with overlapping empty states wavefunctions. The 4.5% Co content in our samples lies below the percolation threshold. Co doped CeO_2 and Co doped TiO_2 exhibit similarities in terms of

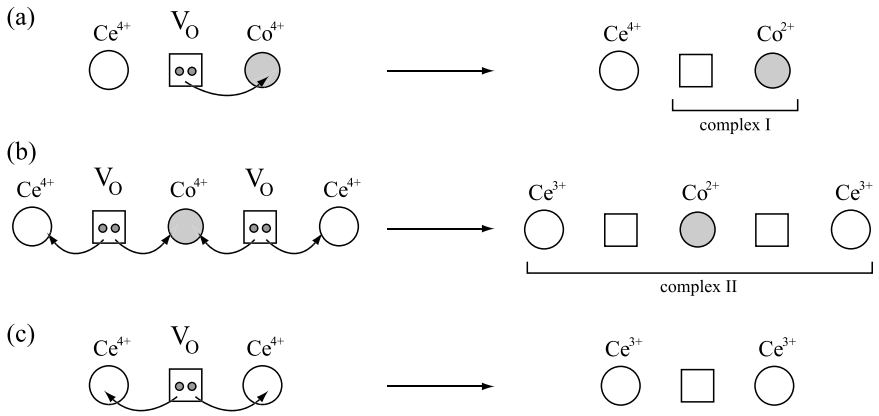

Figure 9. (a) Scheme illustrating the formation of complex I (see the text for details). (b) The same as (a) for complex II. (c) Scheme illustrating the formation of Ce^{3+} ions when an oxygen vacancy is created in the CeO_2 lattice.

charge state of the cations and of the need for local charge compensation. Therefore the mechanism proposed by Kikoin and Fleurov, involving complex I to mediate long range order, may be operative in the present system. The sensitivity of the FM response to oxygen could be linked to the occupancy of the defect band. Further studies should help to clarify this issue and the microscopic picture may be more complicated. Indeed, as discussed in the preceding section, there are a large number of Ce^{3+} ions in the samples. This naturally leads to the question of knowing whether complex II could be involved in the magnetic exchange leading to RT-FM. Fernandes *et al* showed that the amount of Ce^{3+} increases with the Co content in nanocrystalline Co doped $CeO_{2-\delta}$ films electrodeposited on Si [29]. Although a more detailed and systematic investigation as a function of Co concentration is needed in our case, the high concentration of Ce^{3+} and the Ce^{3+}/Co^{2+} ratio ($\sim$10% Ce^{3+} for 4.5% Co) suggest that defects such as complex II could be abundant in the epilayers. The final compound resulting from CeO_2 reduction is Ce_2O_3, with Ce ions in the 3+ charge state. This sesquioxide is antiferromagnetic with a Néel temperature of 9 K and an absolute moment of 2.17 μ_B per Ce_2O_3 molecule [43]. Calculation reproduced this value quite well (2.13 μ_B per Ce_2O_3) assuming that each localized 4f electron of Ce contributes exactly 1 μ_B to the magnetic moment [44]. Therefore, Ce^{3+} ions in Co doped ceria might possibly carry a magnetic moment and contribute to the exchange processes. Although the measured saturation magnetization does not necessarily imply ordering of Ce^{3+} magnetic moments and/or that the band related to oxygen vacancies is spin-polarized, clearly, more experiments as well as calculations are required to get a satisfying microscopic view of the magnetic exchange in Co doped $CeO_{2-\delta}$. The possibility that defects such as complex II may be associated with oxygen vacancies, not localized in the vicinity of Co ions, might be involved in a long range percolative ferromagnetic exchange should stimulate further theoretical and experimental work.

7. Conclusion

Co doped $CeO_{2-\delta}$ thin films were grown by pulsed laser deposition on oxidized Si and $SrTiO_3(001)$ substrates. Structural, magnetic and spectroscopic investigations show that Co doped $CeO_{2-\delta}$ is an intrinsic diluted magnetic oxide with a Curie temperature above 400 K. The ferromagnetic signal depends sensitively on the oxygen pressure during growth and post-growth annealing. Epilayers grown on $SrTiO_3$ have a good crystalline quality and exhibit a strong magnetic anisotropy with an out-of-plane easy axis. X-ray spectroscopies reveal that Co ions are mostly in the divalent Co^{2+} state and a fraction of the Ce ions are in the 3+ charge state. This could indicate that doping with the aliovalent Co^{2+} ions leads to the formation of extended defects associating the magnetic impurities with oxygen vacancies and Ce^{3+} ions in order to preserve locally the charge neutrality. Such extended complexes might be involved in a long range percolative ferromagnetic exchange.

Acknowledgments

We thank M Selmane for his help with x-ray diffraction experiments, I Vickridge and J Siejka for assistance during RBS measurements and A Anane (Unité Mixte de Physique CNRS/Thalès) for helpful discussions. This work was partly supported by the nanoscience and nanotechnology PNANO program of the French Agence Nationale pour la Recherche and by the French-Brazilian CAPES-COFECUB program.

References

[1] Haghiri-Gosnet A M and Renard J P 2003 *J. Phys. D: Appl. Phys.* **36** R127
[2] Eerenstein W, Mathur N D and Scott J F 2006 *Nature* **442** 759
[3] Dietl T, Ohno H, Matsukura F, Cibert J and Ferrand D 2000 *Science* **287** 1019
[4] Matsumoto Y, Murakami M, Shono T, Hasegawa T, Fukumura T, Kawasaki M, Ahmet P, Chikyow T, Koshihara S Y and Koinuma H 2001 *Science* **291** 854
[5] Kaspar T C *et al* 2005 *Phys. Rev. Lett.* **95** 217203
[6] Ueda K, Tabata H and Kawai T 2001 *Appl. Phys. Lett.* **79** 988
[7] Rode K, Anane A, Mattana R, Contour J P, Durand O and LeBourgeois R 2003 *J. Appl. Phys.* **93** 7676
[8] Venkatesan M, Fitzgerald C B, Lunney J G and Coey J M D 2004 *Phys. Rev. Lett.* **93** 177206

[9] Norton D P, Pearton S J, Hebard A F, Theodoropoulou N, Boatner L A and Wilson R G 2003 *Appl. Phys. Lett.* **82** 239
[10] Fitgerald C B, Venkatesan M, Dorneles L S, Gunning R, Stamenov P, Coey J M D, Stampe P A, Kennedy R J, Moreira E C and Sias U S 2006 *Phys. Rev.* B **74** 115307
[11] Ogale S B *et al* 2003 *Phys. Rev. Lett.* **91** 077205
[12] Hong N H, Sakai J, Huong N T, Poirot N and Ruyter A 2005 *Phys. Rev.* B **72** 045336
[13] Hong N H, Poirot N and Sakai J 2006 *Appl. Phys. Lett.* **89** 042503
[14] Philip J, Punnoose A, Kim B I, Reddy K M, Layne S, Holmes J O, Satpati B, Leclair P R, Santos T S and Moodera J S 2006 *Nat. Mater.* **5** 298
[15] Zhao Y G *et al* 2003 *Appl. Phys. Lett.* **83** 2199
[16] Herranz G *et al* 2006 *Phys. Rev. Lett.* **96** 027207
[17] Seshadri R 2005 *Curr. Opin. Solid State Mater. Sci.* **9** 1
[18] Song C, Geng K W, Zeng F, Wang X B, Shen Y X, Pan F, Xie Y N, Liu T, Zhou H T and Fan Z 2006 *Phys. Rev.* B **73** 024405
[19] Jedrecy N, von Bardeleben H J, Zheng Y and Cantin J L 2004 *Phys. Rev.* B **69** 041308
[20] Sati P *et al* 2006 *Phys. Rev. Lett.* **96** 017203
[21] Venkatesan M, Fitzgerald C B and Coey J M D 2004 *Nature* **430** 630
[22] Hong N H, Sakai J, Poirrot N and Brize V 2006 *Phys. Rev.* B **73** 132404
[23] Das Pammaraju C and Sanvito S 2005 *Phys. Rev. Lett.* **94** 217205
[24] Osorio-Guillén J, Lany S, Barabash S V and Zunger A 2006 *Phys. Rev. Lett.* **96** 107203
[25] Coey J M D, Venkatesan M and Fitzgerald C B 2005 *Nat. Mater.* **4** 173
[26] Kikoin K and Fleurov V 2006 *Phys. Rev.* B **74** 174407
[27] Tiwari A, Bhosle V M, Ramachandran S, Sudhakar N, Narayan J, Budak S and Gupta A 2006 *Appl. Phys. Lett.* **88** 142511
[28] Vodungbo B, Zheng Y, Vidal F, Demaille D, Etgens V H and Mosca D H 2007 *Appl. Phys. Lett.* **90** 062510
[29] Fernandes V, Klein J J, Mattoso N, Mosca D H, Silveira E, Ribeiro E, Schreiner W H, Varalda J and de Oliveira A J A 2007 *Phys. Rev.* B **75** 121304(R)
[30] Wen Q Y, Zhang H W, Song Y Q, Yang Q H, Zhu H and Xiao J Q 2007 *J. Phys.: Condens. Matter* **19** 246205
[31] Skorodumova N V, Simak S I, Lundqvist B I, Abrikosov I A and Johansson B 2002 *Phys. Rev. Lett.* **89** 166601
[32] Kang J F, Xiong G C, Lian G J, Wang Y Y and Han R Q 1998 *Solid State Commun.* **108** 225
[33] Overbury S H, Huntley D R, Mullins D R, Ailey K S and Radulovic P V 1997 *J. Vac. Sci. Technol.* A **15** 1647
[34] Hamaya K, Watanabe T, Taniyama T, Oiwa A, Kitamoto Y and Yamazaki Y 2006 *Phys. Rev.* B **74** 045201
[35] van Elp J, Wieland J L, Eskes H, Kuiper P, Sawatzky G A, de Groot F M F and Turner T S 1991 *Phys. Rev.* B **44** 6090
[36] Yağci O 1986 *J. Phys. C: Solid State Phys.* **19** 3487
[37] Mullins D R, Overbury S H and Huntley D R 1998 *Surf. Sci.* **409** 307
[38] Ramachandra Rao M S *et al* 2006 *Appl. Phys. Lett.* **88** 142505
[39] O'Handley R C 2000 *Modern Magnetic Materials: Principles and Applications* (New York: Wiley–Interscience)
[40] Mogensen M, Sammes N M and Tompsett G A 2000 *Solid State Ion.* **129** 63
[41] Janisch R and Spaldin N A 2006 *Phys. Rev.* B **73** 035201
[42] Patterson C H 2006 *Phys. Rev.* B **74** 144432
[43] Pinto H, Mintz M H, Melamud M and Shaked H 1982 *Phys. Lett.* **88** 81
[44] Skorodumova N V, Ahuja R, Simak S I, Abrikosov I A, Johansson B and Lundqvist B I 2001 *Phys. Rev.* B **64** 115108